



## OPEN ACCESS

## EDITED BY

Dirk M. Hermann,  
University of Duisburg-Essen, Germany

## REVIEWED BY

Rongchen Huang,  
University of Colorado, United States  
Sarni Rahim,  
Technical University of Malaysia Malacca,  
Malaysia

## \*CORRESPONDENCE

Xin Huang  
✉ 2017103020035@whu.edu.cn

†These authors have contributed equally to  
this work

RECEIVED 06 August 2024

ACCEPTED 25 March 2025

PUBLISHED 10 April 2025

## CITATION

Zhong Y-L, Liu H and Huang X (2025)  
Genetic mechanisms of dynamic functional  
connectivity density in diabetic retinopathy  
brains: a combined transcriptomic  
and resting-state functional magnetic  
resonance imaging study.  
*Front. Cell. Neurosci.* 19:1476038.  
doi: 10.3389/fncel.2025.1476038

## COPYRIGHT

© 2025 Zhong, Liu and Huang. This is an  
open-access article distributed under the  
terms of the [Creative Commons Attribution  
License \(CC BY\)](#). The use, distribution or  
reproduction in other forums is permitted,  
provided the original author(s) and the  
copyright owner(s) are credited and that the  
original publication in this journal is cited, in  
accordance with accepted academic  
practice. No use, distribution or reproduction  
is permitted which does not comply with  
these terms.

# Genetic mechanisms of dynamic functional connectivity density in diabetic retinopathy brains: a combined transcriptomic and resting-state functional magnetic resonance imaging study

Yu-Lin Zhong<sup>1†</sup>, Hao Liu<sup>2†</sup> and Xin Huang<sup>1\*</sup>

<sup>1</sup>Department of Ophthalmology, Jiangxi Provincial People's Hospital, The First Affiliated Hospital of Nanchang Medical College, Nanchang, Jiangxi, China, <sup>2</sup>School of Ophthalmology and Optometry, Jiangxi Medical College, Nanchang University, Nanchang, Jiangxi, China

**Background:** Diabetic retinopathy (DR) is a condition characterized by fundus lesions resulting from retinal microvascular leakage and obstruction linked to chronic progressive diabetes mellitus. Previous neuroimaging research has revealed both structural and functional changes in the brains of DR patients. Nevertheless, the variations in dynamic functional connectivity density (dFCD) within the brains of DR patients, along with the underlying molecular mechanisms connected to these changes, have yet to be fully understood.

**Methods:** Forty-seven diabetic retinopathy (DR) patients and 46 healthy controls (HCs) matched for sex, age, and education were recruited for this study from the Department of Ophthalmology at the Jiangxi Provincial People's Hospital. All subjects underwent resting-state functional magnetic resonance imaging scans to analyze the differences in dFCD between the two groups. Utilizing the Allen Human Brain Atlas, we conducted spatial correlation analyses integrating transcriptomic and neuroimaging data to pinpoint genes showing correlated expression levels with dFCD alterations in DR patients. Subsequently, we carried out gene enrichment, specific expression, and protein-protein interaction analyses.

**Results:** In comparison to the HC group, the DR group exhibited significantly reduced dFCD variability in the left anterior cingulum, left superior occipital gyrus, and right postcentral gyrus. The abnormal dFCD variability is linked to 1,318 positively and 1,318 negatively associated genes, primarily enriched for biological functions such as ion channels, synapses, and cellular junctions. Specific expression analysis revealed that these genes were distinctly expressed in Purkinje neurons, cortex, and striatum brain regions. Furthermore, protein-protein interaction (PPI) analyses indicated that these positive and negative genes could organize PPI networks with the support of respective hub genes.

**Conclusion:** our study identified altered dFCD variability in brain regions linked to visual and cognitive functions in DR patients. Moreover, transcriptome-neuroimaging correlation analyses revealed a spatial association between these dFCD changes and the genes with unique functional profiles. These genes were

enriched in biologically significant functions and pathways, specific to certain cells and brain areas. Our research offers novel understandings of the genetic mechanisms influencing dFCD alterations in DR.

#### KEYWORDS

diabetic retinopathy, dynamic functional connectivity density, allen human brain atlas, gene expression, rs-fMRI

## Introduction

Diabetes mellitus (DM) is a prevalent metabolic disorder associated with various microvascular complications (Xu, 2015; Bahtiyar et al., 2016; Bansal et al., 2023), among these, DR is a significant microvascular complication affecting the retina in diabetic individuals and stands as a leading cause of global blindness (Wong et al., 2016). A survey conducted in 2020 revealed a worldwide DR prevalence of 22.27% in diabetic populations, impacting approximately 103.12 million individuals (Teo et al., 2021). Risk factors for DR include hypertension, dyslipidemia, obesity, pregnancy, and prolonged diabetes duration (Lopes de Faria et al., 2011; Ting et al., 2016; Wondmeneh and Mohammed, 2024). The primary pathological manifestations of DR encompass capillary non-perfusion, vascular leakage, and degeneration, progressing to proliferative retinal detachment and eventual vision loss. Notably, retinal vessels share similarities in anatomy, physiology, and embryology with cerebral vasculature (Kwa et al., 2002; van de Kreeke et al., 2018). Notably, retinal vessels share similarities in anatomy, physiology, and embryology with cerebral vasculature (Hägg et al., 2013; Sanahuja et al., 2016). Individuals with DR face heightened susceptibility to dementia and Alzheimer's disease (Ciudin et al., 2017; Biessels and Despa, 2018), and potential cognitive impairment (Crosby-Nwaobi et al., 2013; Chai et al., 2024). While evidence indicates brain alterations and abnormal central nervous system (CNS) activity in DR patients, the underlying neurophysiological mechanisms necessitate further exploration.

Resting-state functional magnetic resonance imaging (rs-fMRI), a non-invasive imaging technique, enables the examination of spontaneous intrinsic brain activity by measuring fluctuations in blood oxygen level-dependent (BOLD) signals without specific tasks or stimuli (Fox and Raichle, 2007; Barkhof et al., 2014). Studies using resting-state functional MRI have revealed diverse patterns of spontaneous brain activity alterations in DR patients, including amplitude of low-frequency fluctuations (ALFF), dynamic ALFF (dALFF), regional homogeneity (ReHo), and functional network connectivity (FNC), predominantly observed in brain regions like the middle occipital gyrus, calcarine, anterior cingulate gyrus, posterior cerebellar lobe, and networks associated with visual and cognitive functions (e.g., visual network, default mode network, executive control network, and salience network). These findings shed light on the neural mechanisms underlying visual and central nervous system abnormalities in DR (Huang et al., 2019, 2020, 2021a; Liao X.-L. et al., 2019; Qi et al., 2020; Shi et al., 2022). Functional connectivity density (FCD) analysis, an extension of the FC method, assesses the importance

of network nodes in functional integration by measuring their total connectivity strength with all other nodes in the brain network (Lv et al., 2018; Tomasi and Volkow, 2010). This approach, without requiring prior assumptions, is suited for exploratory analyses (Tomasi et al., 2016; Pang et al., 2017; Zhang et al., 2017). Moreover, the human brain is a complex dynamic system with non-stationary neural activity and constantly changing neural interactions (Hutchison et al., 2013; Calhoun et al., 2014; Liao W. et al., 2019), implying the importance of investigating dynamic neural communication across different brain regions in DR patients utilizing the dFCD approach. However, the specific alterations in dFCD among DR patients remain unclear.

DR has a hereditary component, with estimated heritability ranging from 6 to 33% (Kim et al., 2022). Multiple studies have demonstrated familial clustering of DR (Zhang et al., 2010; Cho and Sobrin, 2014), with notably high concordance rates among family members; 65% in twins with type 1 diabetes and 95% in twins with type 2 diabetes (Leslie and Pyke, 1982). These findings imply the genetic regulation of DR onset and severity. Genome-wide association studies (GWAS) have the potential to identify genetic risk loci associated with DR. A comprehensive meta-analysis has revealed several gene loci linked to DR that are crucial for cell survival, insulin signaling, and angiogenesis (Grassi et al., 2011). Moreover, various studies have highlighted the influence of genetic factors on resting-state brain function (Fornito et al., 2011). Nevertheless, the genetic underpinnings of neuroimaging changes in DR patients are not effectively captured by GWAS. This challenge is compounded by the fact that most loci identified by GWAS are situated in regulatory, rather than coding, regions of the genome, posing significant challenges for their biological interpretation (Edwards et al., 2013; Tam et al., 2019). Spatial correlation analyses integrating transcriptomics and neuroimaging data from the Allen Human Brain Atlas (AHBA), known for its case-control imaging discrepancies, were conducted to explore the genetic basis of macroscopic neuroimaging alterations (Arnatkeviciute et al., 2022; Xue et al., 2022). This method is widely used to unveil gene expression patterns associated with structural and functional variations in patients' brains, although investigations on the genetic mechanisms underlying dFCD changes in DR are lacking.

Therefore, In our study, we initially assessed and compared dFCD differences between DR patients and controls. Subsequently, utilizing gene expression data from the AHBA database integrated with dFCD maps, we conducted spatial correlation analyses to identify genes whose expression levels correlated with dFCD changes in DR. Finally, gene enrichment, specific expression, and protein-protein interaction analyses were carried out on the

identified genes to elucidate their functions and understand the molecular mechanisms behind dFCD alterations in DR.

## Materials and methods

### Participants

Forty-seven diabetic retinopathy (DR) patients and 46 healthy controls (HCs) matched for sex, age, and education were recruited for this study from the Department of Ophthalmology at the Jiangxi Provincial People's Hospital.

The inclusion criteria for diabetic retinopathy (DR) were as follows: (1) Fasting blood glucose levels of equal to or greater than 7.0 mmol/L, random blood glucose levels of equal to or greater than 11.1 mmol/L, or 2-h glucose levels of equal to or greater than 11.1 mmol/L; (2) All DR patients were diagnosed with non-proliferative DR without macular edema. The DR classification followed the Early Treatment Diabetic Retinopathy Study grading scheme, encompassing mild and moderate non-proliferative DR, severe non-proliferative retinopathy, and non-high-risk and high-risk proliferative DR.

The exclusion criteria for diabetic retinopathy (DR) were as follows: (1) Patients with proliferative DR complicated by retinal detachment and vitreous hemorrhage; (2) Presence of additional ocular complications (such as cataracts, glaucoma, high myopia, or optic neuropathy); (3) Patients diagnosed with diabetic nephropathy (urine albumin/creatinine ratio > 30 mg/g persisting for more than 3 months); (4) Diabetic neuropathy.

The inclusion and exclusion criteria for healthy controls (HC) were as follows: (1) Fasting blood glucose levels < 7.0 mmol/L, random blood glucose levels < 11.1 mmol/L, glycosylated hemoglobin levels < 6.5%; (2) Absence of ocular diseases (such as myopia, cataracts, glaucoma, optic neuritis, or retinal degeneration); (3) Binocular visual acuity  $\geq$  1.0; (4) No history of ocular surgery; (5) Absence of psychiatric disorders. All participants met the eligibility criteria for MRI scans.

The study protocol adhered to the Declaration of Helsinki and received approval from the Research Ethics Committee of Jiangxi Provincial People's Hospital. Before participating in the study, all participants were informed about the study's objectives, methods, and potential risks, and provided written informed consent to participate.

### MRI acquisition

Functional images were acquired using a gradient-echo-planar imaging sequence. Participants were instructed to maintain a relaxed state with closed eyes, refrain from focusing on specific thoughts, and avoid falling asleep. Whole-brain T1-weighted images were obtained through a three-dimensional brain volume imaging (3D-BRAVO) MRI protocol with the following parameters: repetition time (TR)/echo time (TE) = 8.5/3.3 ms, slice thickness = 1.0 mm, no intersection gap, acquisition matrix = 256  $\times$  256, field of view = 240  $\times$  240 mm<sup>2</sup>, and flip angle = 12°. Functional images were acquired using a gradient-echo-planar imaging sequence with the following parameters:

TR/TE = 2,000 ms/25 ms, slice thickness = 3.0 mm, gap = 1.2 mm, acquisition matrix = 64  $\times$  64, flip angle = 90°, field of view = 240  $\times$  240 mm<sup>2</sup>, voxel size = 3.6  $\times$  3.6  $\times$  3.6 mm<sup>3</sup>, and 35 axial slices. All participants were instructed to relax with closed eyes, avoiding specific thoughts or falling asleep.

### Data preprocessing

The preprocessing steps utilized the Data Processing and Analysis of Brain Imaging (DPABI) toolbox (DPABI)<sup>1</sup> (Yan et al., 2016), a tool based on Statistical Parametric Mapping (SPM12) incorporated in MATLAB 2013a (MathWorks, Natick, MA, United States). The pre-processing protocol consisted of the following steps: (1) Removal of the initial 10 volumes, (2) Correction for slice timing effects and motion, excluding participants with head motion exceeding 2 mm or rotation exceeding 1.5° during scanning (Van Dijk et al., 2012). (3) Normalization of data to Montreal Neurological Institute (MNI) 152 space at a resolution of 3 mm  $\times$  3 mm  $\times$  3 mm, and (4) Spatial smoothing through convolution with a 6 mm  $\times$  6 mm  $\times$  6 mm isotropic Gaussian kernel at full width at half maximum.

### Dynamic functional connectivity density analysis

The analysis of dFCD was processed with the DynamicBC software. dFCD analysis was conducted using the sliding-window approach, with a window size of 50 TR and a sliding step of 10 TR. We obtained a global FCD map in each window by computing Pearson's correlations between the truncated time course of all pairs of voxels within the automated anatomical labeling-90 (AAL-90) atlas (comprising 45 cortical and subcortical regions in each hemisphere) (Tzourio-Mazoyer et al., 2002), yielding a set of sliding-window FCD maps for each subject. We used  $r = 0.2$  as the correlation coefficient threshold to define the connectivity between two voxels. If their correlation coefficient was larger than 0.2, then connectivity was present between them. The threshold was selected to eliminate the weak correlations induced by noise (Li et al., 2019). Subsequently, the temporal variability was estimated by computing the SD of FCD across sliding windows. In consideration that the global signal regression may induce controversial negative correlations (Fox et al., 2009; Murphy et al., 2009), all our analyses were performed based on positive correlation above a threshold of 0.2.

### Brain gene expression data processing

Brain gene expression data were obtained from the AHBA dataset<sup>2</sup>, which was derived from six human postmortem donors. The original expression data of more than 20,000 genes at 3,702 spatially distinct brain tissue samples were processed using a newly

1 <http://www.rfmri.org/dpabi>

2 <http://www.brainmap.org>

proposed pipeline (Arnatkeviciute et al., 2019). The dataset from AHBA was processed following recommendations from previous studies to ensure consistency and reproducibility of results. Partial Least Squares (PLS) regression was employed to investigate the regional dFCD maps in relation to the transcriptional activity of all 10,027 genes.

### Gene enrichment analysis

Gene enrichment analysis was performed utilizing the DAVID Functional Annotation Bioinformatics Microarray Analysis platform, accessible at <https://metascape.org/gp/index.html#/main/step1>. Gene Ontology (GO) was employed to assess biological functions, covering biological processes (BP), cellular components (CC), and molecular functions (MF). Pathway databases, particularly the Kyoto Encyclopedia of Genes and Genomes (KEGG) pathway, were utilized to evaluate pertinent biological pathways. Enrichment analysis plots were created with SRplot available at <http://www.bioinformatics.com.cn/>.

### Specific expression analysis

Cell type-specific expression analysis, brain region-specific expression analysis, and temporal-specific expression analyses were performed at [doughertytools.wustl.edu/CSEAtool.html](http://doughertytools.wustl.edu/CSEAtool.html) to identify the distinct cell types, brain regions, and developmental stages showing an overrepresentation of these genes. A specificity index probability (pSI) was utilized with two thresholds (0.01 and 0.001) to evaluate the enrichment of genes in specific terms relative to others.

### Protein-protein interaction analysis

Protein-protein interaction (PPI) analysis was conducted using STRING v11.0<sup>3</sup> to explore whether genes linked to brain functional alterations could form a PPI network. PPI pairs with a confidence interaction score > 0.9 were extracted for analysis. Hub genes were

<sup>3</sup> <https://string-db.org/>

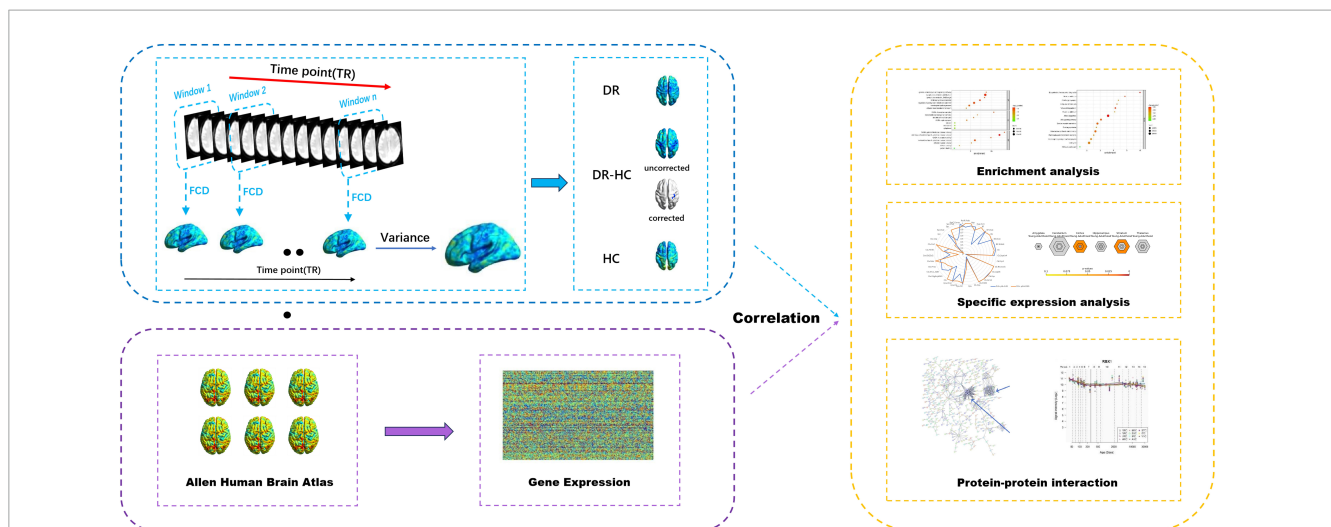


FIGURE 1

Overview of the analysis pipeline. Sliding window method was utilized to compute dFCD, the dFCD in the DR and HC groups were obtained by one-sample *t*-tests, and the dFCD differences between the two groups were compared by two-sample *t*-tests. Then the association between dFCD differences and gene expression from the AHBA was explored. Afterward, enrichment analysis, specific expression analysis and protein-protein interaction analysis were performed on this basis. dFCD, dynamic functional connectivity density; DR, diabetic retinopathy; HC, health control; AHBA, Allen Human Brain Atlas.

TABLE 1 Demographics and visual measurements between two groups.

Condition	DR group	HC group	$t/\chi^2$	P
Gender (male/female)	26/21	24/22	0.093	0.76
Age (years)	54.84 ± 3.22	55.36 ± 4.48	-0.462	0.65
Duration (months)	11.54 ± 4.37	-	-	-
Education	11.88 ± 2.05	11.68 ± 2.60	0.296	0.77
BCVA-OD	0.66 ± 0.15	1.11 ± 0.12	-11.523	<0.001*
BCVA-OS	0.64 ± 0.14	1.05 ± 0.18	-8.967	<0.001*
MoCA	25.37 ± 0.58	25.20 ± 0.74	0.927	0.358

BCVA, best corrected visual acuity; OD, oculus dexter; OS, oculus sinister; MoCA, Montreal Cognitive Assessment. \*Means a significant difference.

identified as those within the top 15% of degree values, representing the number of edges connected to a gene. Furthermore, the Human Brain Transcriptome database<sup>4</sup> was utilized to delineate the spatial-temporal expression trajectory of hub genes exhibiting the highest degree values.

An overview of the analysis pipeline is illustrated in Figure 1.

### Statistical analysis

The demographic and clinical characteristics of the groups were analyzed using SPSS version 20.0 software (SPSS Inc.,

Chicago, IL, United States), employing the Chi-square test and independent-samples *t*-test, with a *p*-value of less than 0.05 considered indicative of a significant statistical difference. Intragroup patterns of dFCD maps were assessed through one-sample *t*-tests using SPM8 software.

Furthermore, two-sample *t*-tests were conducted to investigate group disparities in the dFCD maps (50TRs), employing the Gaussian random field (GRF) method for correcting multiple comparisons. Age and sex were regressed as covariates, and the analysis was performed with SPM8 software at a voxel level of  $p < 0.001$  with GRF correction and a cluster level of  $p < 0.05$ .

Additionally, partial least squares (PLS) regression was utilized to explore the relationship between regional changes in dFCD and transcriptional activity for all 10,027 genes.

4 <http://hbatlas.org/>

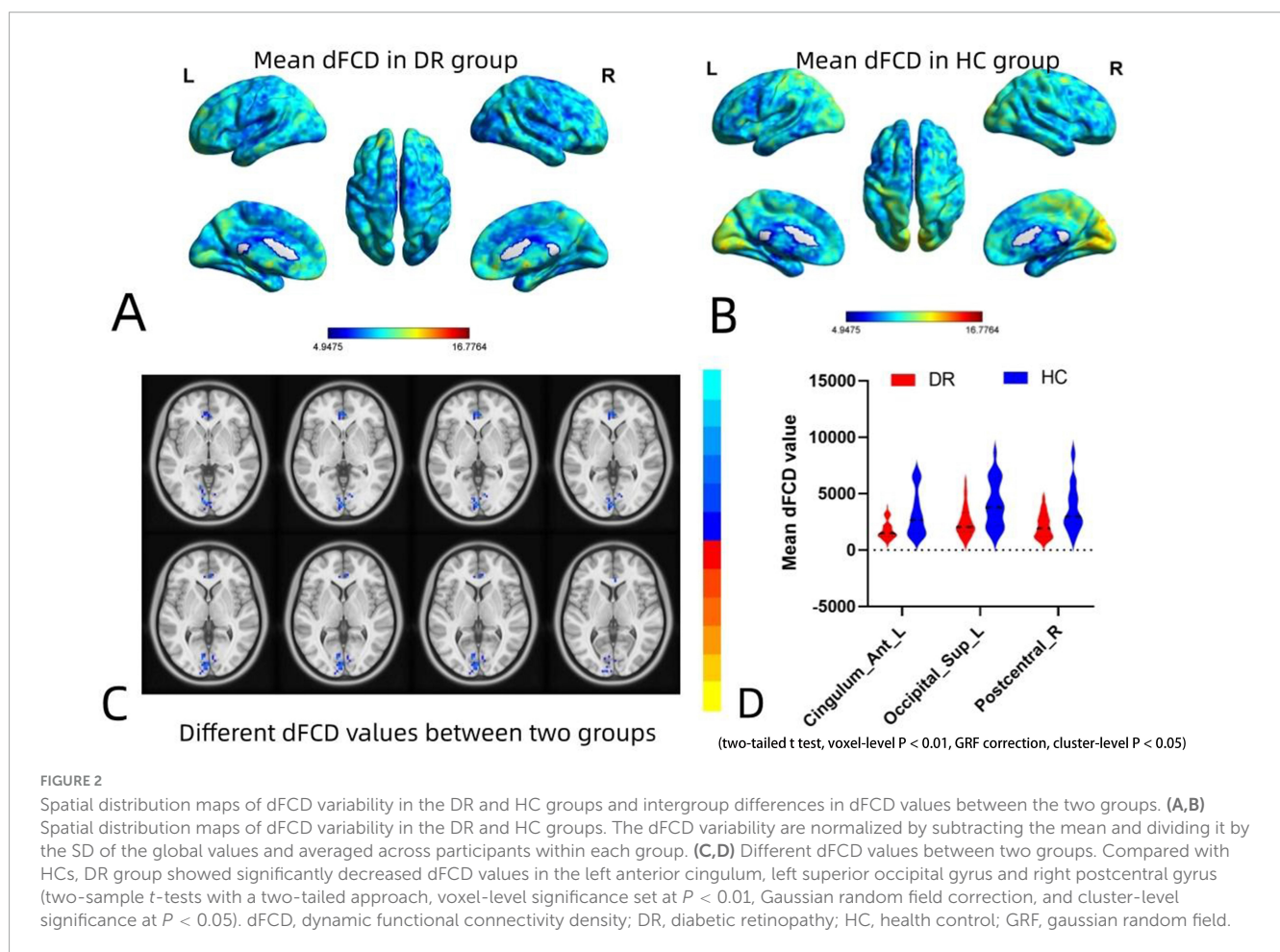


TABLE 2 Group differences in dFCD variability between DR patients and HCs.

Brain regions	MNI coordinates			Peak <i>t</i> -values	Cluster size
	x	y	z		
<b>DR &lt; HC</b>					
Cingulum_Ant_L	-9	36	-6	-4.3492	67
Occipital_Sup_L	-12	-99	9	-4.5470	82
Postcentral_R	33	-30	51	-4.8415	78

dFCD, dynamic functional connectivity density; MNI, Montreal Neurologic Institute; DR, diabetic retinopathy; HC, health control; R, right; L, left; Ant, anterior; Sup, superior.

## Results

### Demographic and clinical characteristics

Significant differences were observed in best-corrected visual acuity ( $P < 0.001$ ) between the two groups. However, there were no significant differences in sex, age, or body mass index between the two groups. Further details are provided in Table 1.

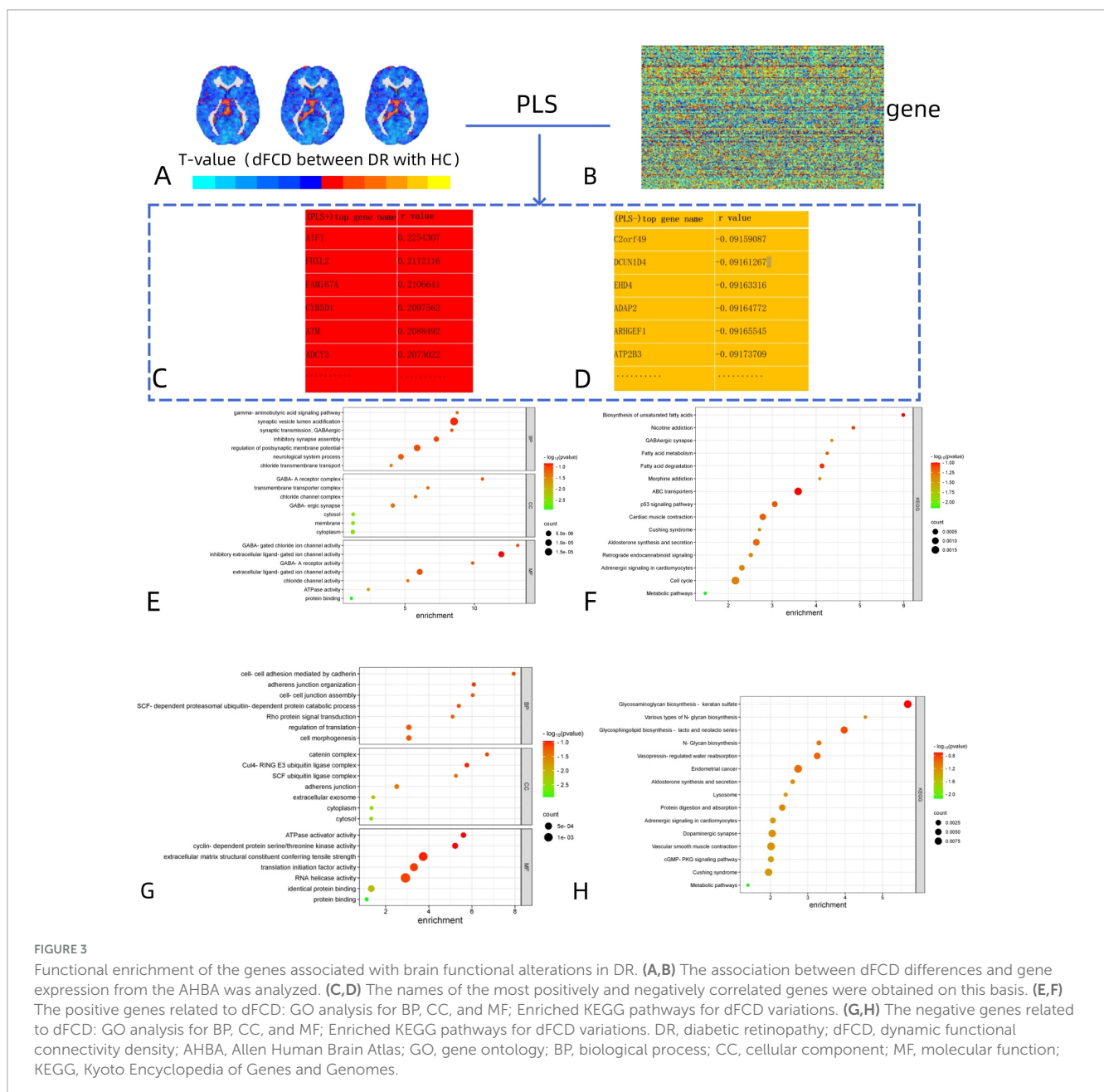
### Differences in dFCD variability between DR and HC

The spatial distribution of dFCD variability in the DR group and the HC group is shown in Figures 2A,B. The results of

the two-sample  $t$ -tests indicate that, compared to the HC group, the DR group exhibited significantly decreased dFCD values in the left anterior cingulum, left superior occipital gyrus and right postcentral gyrus (two tailed, voxel level of  $p < 0.001$  with GRF correction and a cluster level of  $p < 0.05$ ) (Figures 2C,D; Table 2).

### Gene enrichment results

To elucidate the biological functions and pathways associated with brain functional alterations, the  $t$ -values of dFCD maps (Figure 3A) between two groups and gene (Figure 3B) was analyzed. we conducted functional enrichment analyses. For the positive genes related to dFCD, there were a total of 1,318 genes (Figure 3C). Gene Ontology (GO) analysis revealed 7



biological processes (BP), including gamma-aminobutyric acid signaling pathway, synaptic vesical lumen acidification, synaptic transmission GABAergic, inhibitory synapse assembly, regulation of postsynaptic membrane potential, neurological system process, and chloride transmembrane transport. Additionally, 7 cellular components (CC) were identified, such as GABA-A receptor complex, transmembrane transporter complex, chloride channel complex, GABA-ergic synapse, cytosol, membrane, and cytoplasm. Moreover, 7 molecular functions (MF) were annotated, including GABA-gated chloride ion channel activity, inhibitory extracellular

ligand-gated ion channel activity, GABA-A receptor activity, extracellular ligand-gated ion channel activity, chloride channel activity, ATPase activity, and protein binding (Figure 3E). In terms of KEGG pathways, 15 pathways were enriched, including Biosynthesis of unsaturated fatty acids, Nicotine addiction, GABAergic synapse and Fatty acid metabolism, etc. (Figure 3F).

For the negative genes related to dFCD, there were also 1,318 genes identified (Figure 3D). GO analysis revealed 7 biological processes, such as cell-cell adhesion mediated by cadherin, adherens junction organization, cell-cell junction

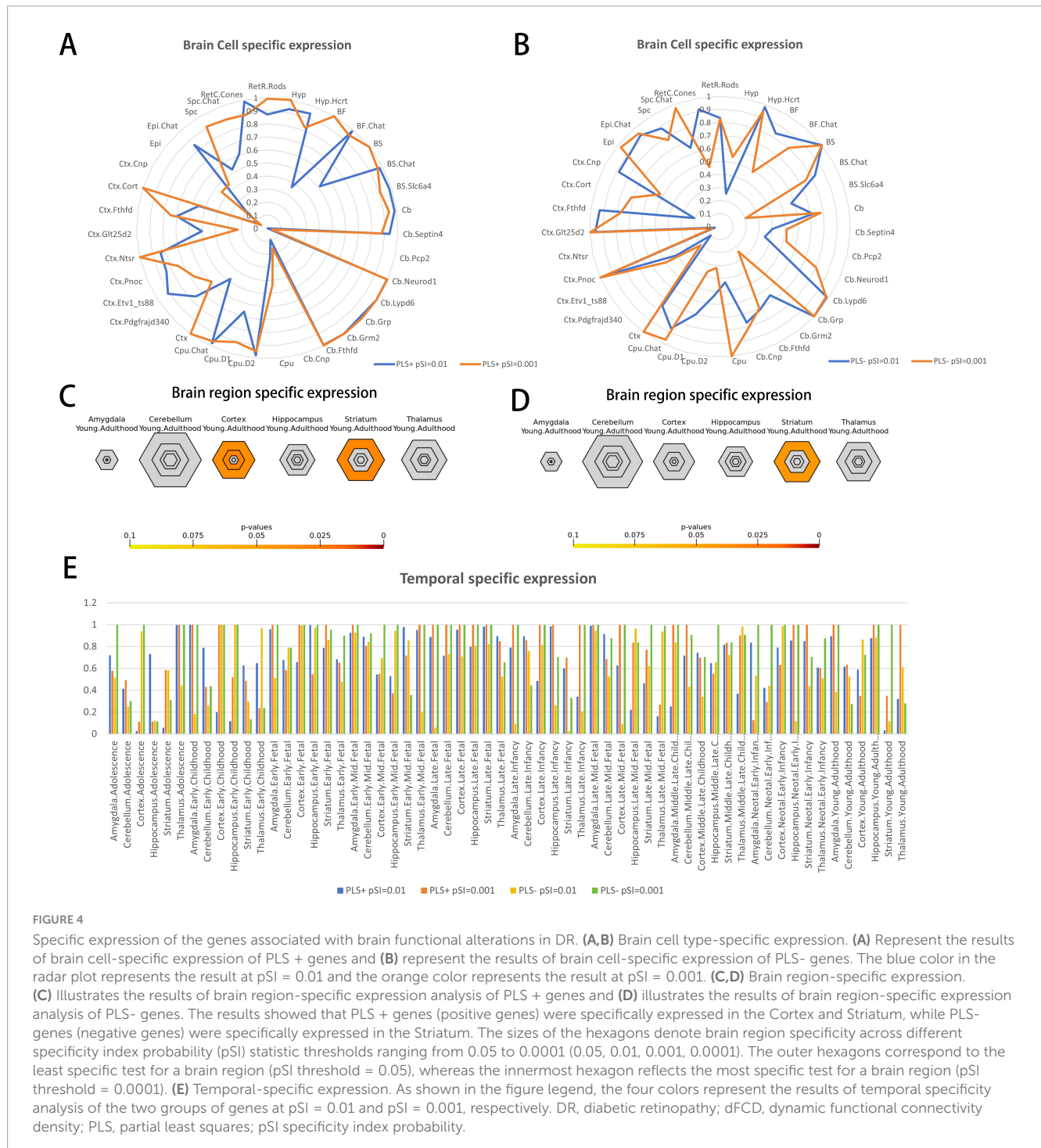


TABLE 3 Brain cell type specific expression results.

Brain cell types and <i>P</i> -values	PLS + pSI = 0.01	PLS + pSI = 0.001	PLS- pSI = 0.01	PLS- pSI = 0.001
RetR.Rods	0.872	0.992	0.834	0.826
Hyp	0.927	1	0.257	0.543
Hyp.Hcrt	0.938	0.823	0.98	0.946
BF	0.366	1	0.833	0.487
BF.Chat	0.988	0.948	0.893	0.802
BS	0.515	1	1	1
BS.Chat	0.977	0.96	0.828	0.747
BS.Slc6a4	0.982	0.907	0.575	0.208
Cb	0.983	0.94	0.72	0.779
Cb.Septin4	0.937	0.878	0.402	0.512
Cb.Pcp2	0.002	0.039	0.353	0.523
Cb.Neurod1	0.997	1	0.512	0.802
Cb.Lypd6	0.999	1	0.982	0.976
Cb.Grp	0.984	1	0.998	1
Cb.Grm2	0.999	1	0.652	0.239
Cb.Fthfd	0.992	0.997	0.709	0.697
Cb.Cnp	0.091	0.158	0.767	0.812
Cpu	0.236	0.438	0.43	1
Cpu.D2	0.978	0.946	0.537	0.32
Cpu.D1	0.663	0.903	0.701	0.358
Cpu.Chat	0.977	0.961	0.868	0.965
Ctx	0.479	1.000	0.753	1
Ctx.Pdgfrjd340	0.755	0.590	0.1	0.209
Ctx.Etv1_ts88	0.910	0.670	0.405	0.501
Ctx.Pnoc	0.839	0.738	0.952	1
Ctx.Ntsr	0.839	1.000	0.041	0.061
Ctx.Glt25d2	0.501	0.227	0.958	1
Ctx.Fthfd	0.698	0.746	0.932	0.771
Ctx.Cort	0.551	1.000	0.209	0.717
Ctx.Cnp	0.074	0.053	0.881	0.521
Epi	0.208	0.446	0.889	0.974
Epi.Chat	0.848	0.446	0.929	0.948
Spc	0.524	0.908	0.877	0.774
Spc.Chat	0.609	0.890	0.646	0.971
RetC.Cones	0.987	0.885	0.913	0.465

PLS, partial least squares; pSI specificity index probability.

assembly, SCF-dependent proteasomal ubiquitin-dependent protein catabolic process, Rho protein signal transduction, regulation of translation, and cell morphogenesis. Additionally, 7 cellular components and 7 molecular functions were identified (Figure 3G), along with 15 enriched KEGG pathways, including Glycosaminoglycan biosynthesis-keratan sulfate, Various types of N-glycan biosynthesis, and Glycosphingolipid biosynthesis-lacto and neolacto series, etc. (Figure 3H).

## Specific expression analysis

For the 1,318 positive genes associated with dFCD, cell-specific expression analysis revealed their distinct expression across various cell types, notably in Cb.Pcp2 (Figure 4A; Table 3). Moreover, brain-specific expression analysis highlighted their specific expression patterns in different brain regions, particularly in the Cortex and Striatum (Figure 4C; Table 4). Temporal-specific expression

TABLE 4 Brain region specific expression results.

Brain regions and development and $p$ -values	PLS + pSI = 0.01	PLS + pSI = 0.001	PLS- pSI = 0.01	PLS- pSI = 0.001
Amygdala.young.adulthood	0.396	1	0.154	1
Cerebellum.young.adulthood	0.582	0.985	0.315	0.594
Cortex.young.adulthood	0.005	0.585	0.922	0.868
Hippocampus.young.adulthood	0.586	0.62	0.981	0.964
Striatum.young.adulthood	0.392	0.448	0.067	0.942
Thalamus.young.adulthood	0.637	0.896	0.363	0.9

PLS, partial least squares; pSI specificity index probability.

analysis further elucidated their differential expression across developmental stages and brain regions, however, no significant differential expression was found in this study (Figure 4E; Table 5).

In contrast, cell-specific expression analysis of the 1,318 negative genes linked to dFCD did not reveal significant expression (Figure 4B; Table 3). Brain-specific expression analysis showcased their distinct expression in different brain regions, notably in the Striatum (Figure 4D; Table 4). Temporal-specific expression analysis delineated their varied expression across developmental stages and brain regions, similar to the positive genes, we did not find significant differential expression (Figure 4E; Table 5).

## PPI network and hub genes

PPI analysis uncovered that 1,318 positive genes linked to dFCD formed an interlinked PPI network (Figure 5A). Additionally, we elucidated the spatial-temporal expression patterns of three key genes with the highest degree values: RBX1 (Figure 5B), DDB2 (Figure 5C), and CBX2 (Figure 5D).

Similarly, PPI analysis revealed that 1,318 negative genes associated with dFCD constructed an interconnected PPI network (Figure 6A). We further outlined the spatial-temporal expression trajectories of three pivotal genes with the highest degree values: RBX1 (Figure 6B), DCAF13 (Figure 6C), and CUL4A (Figure 6D).

## Discussion

This study represents an innovative approach integrating functional magnetic resonance imaging with transcriptome-neuroimaging spatial correlation to explore the genetic underpinnings of dFCD variability in diabetic retinopathy (DR). Our investigation revealed a significant reduction in dFCD variability within the left anterior cingulum, left superior occipital gyrus, and right postcentral gyrus in the DR group compared to the healthy control (HC) group. Transcriptome-neuroimaging correlation analyses identified two groups of DR-related genes (PLS1 + and PLS1-) that exhibited substantial enrichment in biological functions and pathways related to ion channels, synaptic function, neuronal systems, and cellular junctions. Specific expression analyses indicated the unique expression of these genes in Purkinje neurons, the cortex, and striatum brain regions, with no developmental period-specific expression observed.

Additionally, genes linked to altered brain function were capable of forming a protein-protein interaction (PPI) network supported by hub genes. These insights suggest that the disrupted brain function in DR patients arises from intricate interactions among multiple genes with diverse functional characteristics, offering novel perspectives on the molecular mechanisms linked to dFCD alterations in DR patients.

Significantly reduced dFCD variability was observed in the left anterior cingulum, left superior occipital gyrus, and right postcentral gyrus in the diabetic retinopathy (DR) group compared to the healthy control (HC) group. The anterior cingulate gyrus, a component of the salience network, plays a role in higher functions like attention allocation (Pardo et al., 1990), reward anticipation, decision making, and emotion (Jackson et al., 2006). A study by Liao et al showed significantly reduced ReHo values in the right anterior cingulate gyrus in patients with DR and hypothesized that this reflected dysfunction of the anterior cingulate gyrus (Liao X.-L et al., 2019). Similar to their results, we found significantly reduced dFCD variability in the left anterior cingulate gyrus in DR patients, which may imply anterior cingulate gyrus dysfunction and lead to corresponding cognitive impairment in DR patients. The superior occipital gyrus is located in the occipital lobe and is mainly responsible for the processing of visual information. It has been found that functional connectivity from the bilateral lingual gyrus to the left superior occipital gyrus was reduced in the DR group compared to healthy controls (Huang et al., 2021b), which suggests disrupted connectivity of the visual network and the dorsal visual pathway, and may reflect impaired top-down modulation and visuospatial function in patients with DR. In another study, gray matter density (GMD) in the right occipital lobe of DR patients was significantly lower than that of healthy controls (Wessels et al., 2006). In addition, there is a significant decrease in intra-network functional connectivity (FC) of the visual network (VN) in DR patients (Huang et al., 2020). Combining these studies, we suggest that the reduced dFCD variability in the left superior occipital gyrus may reflect impaired visual function in DR patients. The postcentral gyrus is located in sensorimotor network (SMN) (Chenji et al., 2016), which plays an important role in motion control. One study found reduced local clustering in the postcentral gyrus in DR patients, which correlates with motor speed (van Duinkerken et al., 2016). Postcentral gyrus is closely associated with PVA-related (primary visual areas) spontaneous brain activity (Wang et al., 2008), and their connection affects the processing of spatial visual information (Ringach et al., 1996). We hypothesize that reduced

TABLE 5 Temporal specific expression results.

Brain regions and development and $p$ -values	PLS + $pSI = 0.01$	PLS + $pSI = 0.001$	PLS- $pSI = 0.01$	PLS- $pSI = 0.001$
Amygdala.adolescence	0.72	0.58	0.516	1
Cerebellum.adolescence	0.412	0.491	0.25	0.302
Cortex.adolescence	0.027	0.111	0.939	1
Hippocampus.adolescence	0.73	0.111	0.122	0.113
Striatum.adolescence	0.058	0.585	0.583	0.312
Thalamus.adolescence	0.998	1	0.441	1
Amygdala.early.childhood	1	1	0.182	1
Cerebellum.early.childhood	0.789	0.43	0.259	0.438
Cortex.early.childhood	0.199	1	1	1
Hippocampus.early.childhood	0.117	0.52	1	1
Striatum.early.childhood	0.626	0.486	0.298	0.135
Thalamus.early.childhood	0.647	0.234	0.968	0.237
Amygdala.early.fetal	0.959	1	0.512	1
Cerebellum.early.fetal	0.677	0.585	0.79	0.788
Cortex.early.fetal	0.657	1	0.992	1
Hippocampus.early.fetal	0.997	0.547	0.971	1
Striatum.early.fetal	0.788	1	0.861	0.954
Thalamus.early.fetal	0.683	0.653	0.478	0.899
Amygdala.early.mid.fetal	0.925	1	0.929	1
Cerebellum.early.mid.fetal	0.891	0.806	0.842	0.922
Cortex.early.mid.fetal	0.544	0.551	0.694	1
Hippocampus.early.mid.fetal	0.53	0.373	0.945	1
Striatum.Early.Mid.Fetal	0.977	0.718	0.858	0.355
Thalamus.early.mid.fetal	0.952	1	0.203	1
Amygdala.late.fetal	0.888	1	0.058	1
Cerebellum.late.fetal	0.718	1	0.731	1
Cortex.late.fetal	0.954	1	0.71	1
Hippocampus.late.fetal	0.798	1	0.807	1
Striatum.late.fetal	0.983	1	0.821	1
Thalamus.late.fetal	0.895	0.849	0.525	0.656
Amygdala.late.infancy	0.791	1	0.091	1
Cerebellum.late.infancy	0.896	0.857	0.759	0.443
Cortex.late.infancy	0.485	1	0.815	1
Hippocampus.late.infancy	0.985	1	0.261	0.704
Striatum.late.infancy	0.601	0.699	0.024	0.33
Thalamus.late.infancy	0.342	1	0.207	1
Amygdala.late.mid.fetal	0.99	1	0.945	1
Cerebellum.late.mid.fetal	0.913	0.685	0.527	0.876
Cortex.late.mid.fetal	0.626	1	0.091	1
Hippocampus.late.mid.fetal	0.22	0.835	0.963	0.839
Striatum.late.mid.fetal	0.462	0.769	0.62	1
Thalamus.late.mid.fetal	0.161	0.269	0.938	0.989

(Continued)

TABLE 5 (Continued)

Brain regions and development and $p$ -values	PLS + pSI = 0.01	PLS + pSI = 0.001	PLS- pSI = 0.01	PLS- pSI = 0.001
Amygdala.middle.late.childhood	0.251	1	0.839	1
Cerebellum.middle.late.childhood	0.718	1	0.433	0.906
Cortex.middle.late.childhood	0.742	0.699	0.341	0.704
Hippocampus.middle.late.childhood	0.647	0.551	0.656	1
Striatum.middle.late.childhood	0.817	0.835	0.725	0.839
Thalamus.middle.late.childhood	0.367	0.903	0.985	0.906
Amygdala.neotal.early.infancy	0.835	0.125	0.534	1
Cerebellum.neotal.early.infancy	0.423	0.293	0.441	1
Cortex.neotal.early.infancy	0.79	0.632	0.987	1
Hippocampus.neotal.early.infancy	0.855	1	0.117	1
Striatum.neotal.early.infancy	0.85	1	0.439	0.704
Thalamus.neotal.early.infancy	0.608	0.603	0.51	0.877
Amygdala.young.adulthood	0.896	1	0.384	1
Cerebellum.young.adulthood	0.614	0.634	0.526	0.272
Cortex.Young.Adulthood	0.589	0.349	0.863	0.723
Hippocampus.Young.Adulthood	0.876	1	0.881	1
Striatum.Young.Adulthood	0.034	0.349	0.113	1
Thalamus.Young.Adulthood	0.32	1	0.611	0.281

PLS, partial least squares; pSI specificity index probability.

dFCD variability in the postcentral gyrus of DR patients may cause abnormalities in motor control, such as abnormal eye movements.

Transcription-neuroimaging spatial association analysis is an effective method to study the genetic mechanisms underlying neuroimaging phenotypes in the patient's brain (Zhang et al., 2022), and can identify genes associated with neuroimaging phenotypes (Fornito et al., 2019). Using transcriptional-neuroimaging spatial association analysis, we identified two groups of genes, PLS + and PLS-, which correlate with changes in dFCD in DR patients. Enrichment analyses showed that these genes were mainly enriched for biological functions and pathways such as ion channels, synapses and cellular junctions. It was shown that ion channels are closely related to neuronal growth and differentiation, membrane potential generation, signal transduction and neurotransmitter release (Moody and Bosma, 2005; Smith and Walsh, 2020; Kumar et al., 2016; Hull and Isom, 2018). Alterations in the expression levels of somatostatin (SRIF) or specific SRIF receptors affect the morphology of retinal cell types (i.e., optic rod cells) and may influence transmitter release in photoreceptors by modulating voltage-gated K<sup>+</sup> and Ca<sup>2+</sup> currents, making SRIF a potentially promising drug SRIF for the treatment of DR (Casini et al., 2005). 11-cis-retinal intervention improves aberrant outer retinal ion channel closure, thereby alleviate diabetes-induced outer retinal layer dysfunction (Berkowitz et al., 2012). This implies that ion channels may be an important therapeutic target for DR. Inter-neuronal communication is largely dependent on synaptic function (Pereda, 2014), and in hyperglycemia, both neurochemical (synaptic) and electrical (gap junction) modes of communication between retinal cells are affected (Eleftheriou et al., 2020). Diabetes

causes a cumulative loss of neural dendrites and synapses in the inner retina, which results in significant thinning of the inner plexiform layer (IPL) (Barber et al., 1998). Hyperphosphorylated tau proteins contribute to diabetic retinal neurodegeneration by disrupting synaptic and mitochondrial function in retinal ganglion cells (RGCs) (Zhu et al., 2018). This suggests the importance of synaptic dysfunction in the pathophysiological process of DR. In DR, the blood-retinal barrier (BRB) is disrupted (Xu et al., 2011). Inflammatory cytokine levels are elevated in the vitreous fluid of patients with DR (Daruich et al., 2018), whereas pro-inflammatory cytokines have been found to cause down-regulation of tight junctions in bovine retinal endothelial cells through the NF- $\kappa$ B pathway, and, increase retinal endothelial cell permeability (Aveleira et al., 2010). In the mouse retina, hyperglycemic memory (HGM) induces sustained oxidative stress, mitochondrial membrane potential collapse and fission, adhesion junction disassembly and subsequent vascular leakage after normalization of blood glucose (Lee et al., 2022). The association between disruption of the blood-retinal barrier (BRB) and the down-regulation or disintegration of cellular connections is evident. Conversely, the overexpression of endothelial CYP2J2 preserves the distribution of endothelial tight junctions and adherens junctions in an ANXA1-dependent manner, thus safeguarding the integrity of the BRB and shielding retinal ganglion cells from loss following ischemia-reperfusion injury (Zhao et al., 2022).

The PLS + genes exhibited specific expression mainly in the cortex and striatum, while the PLS- genes showed predominant expression in the striatum, indicating a focus of diabetic retinopathy (DR) effects on the cerebral cortex. Moreover, the

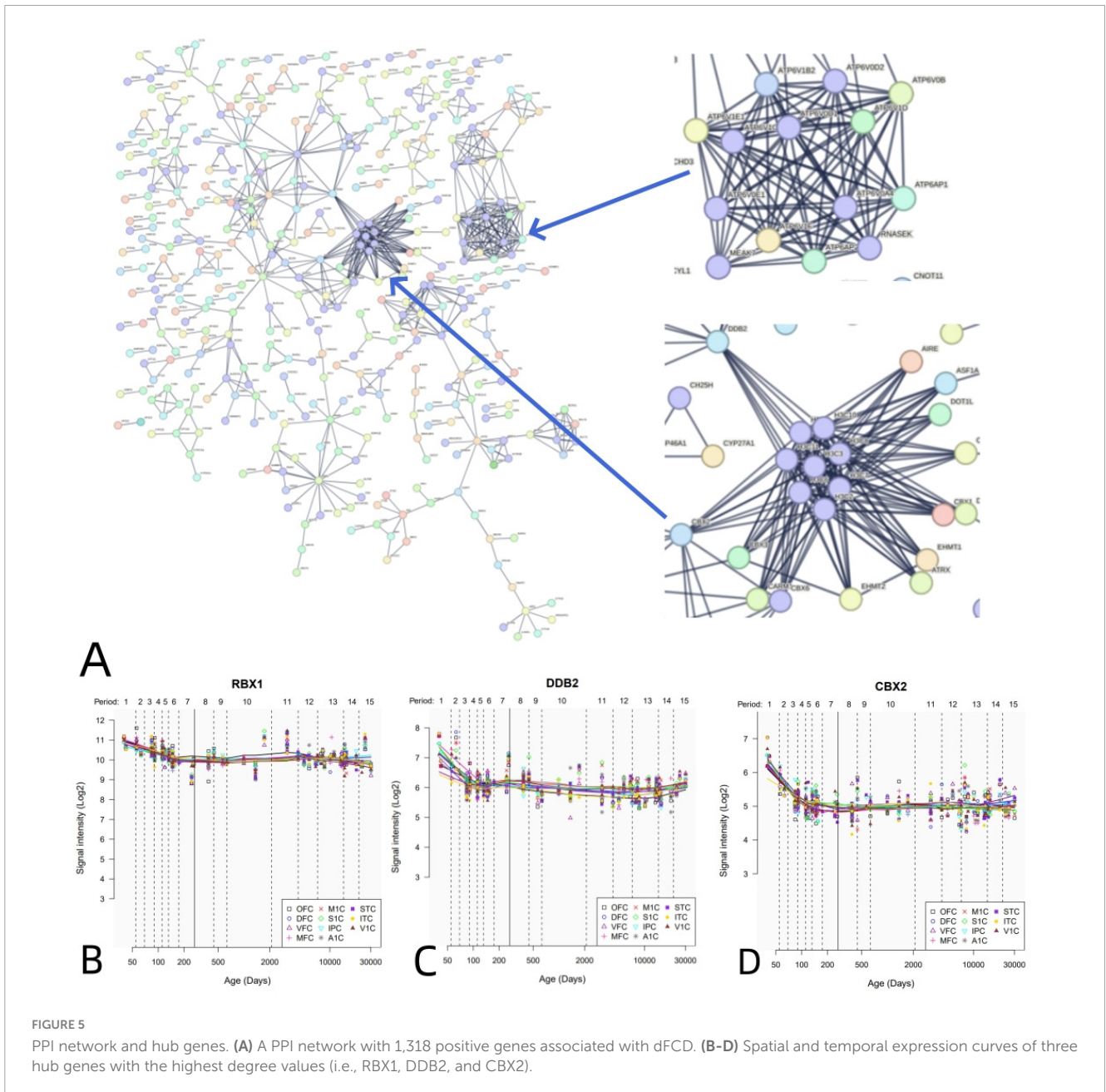
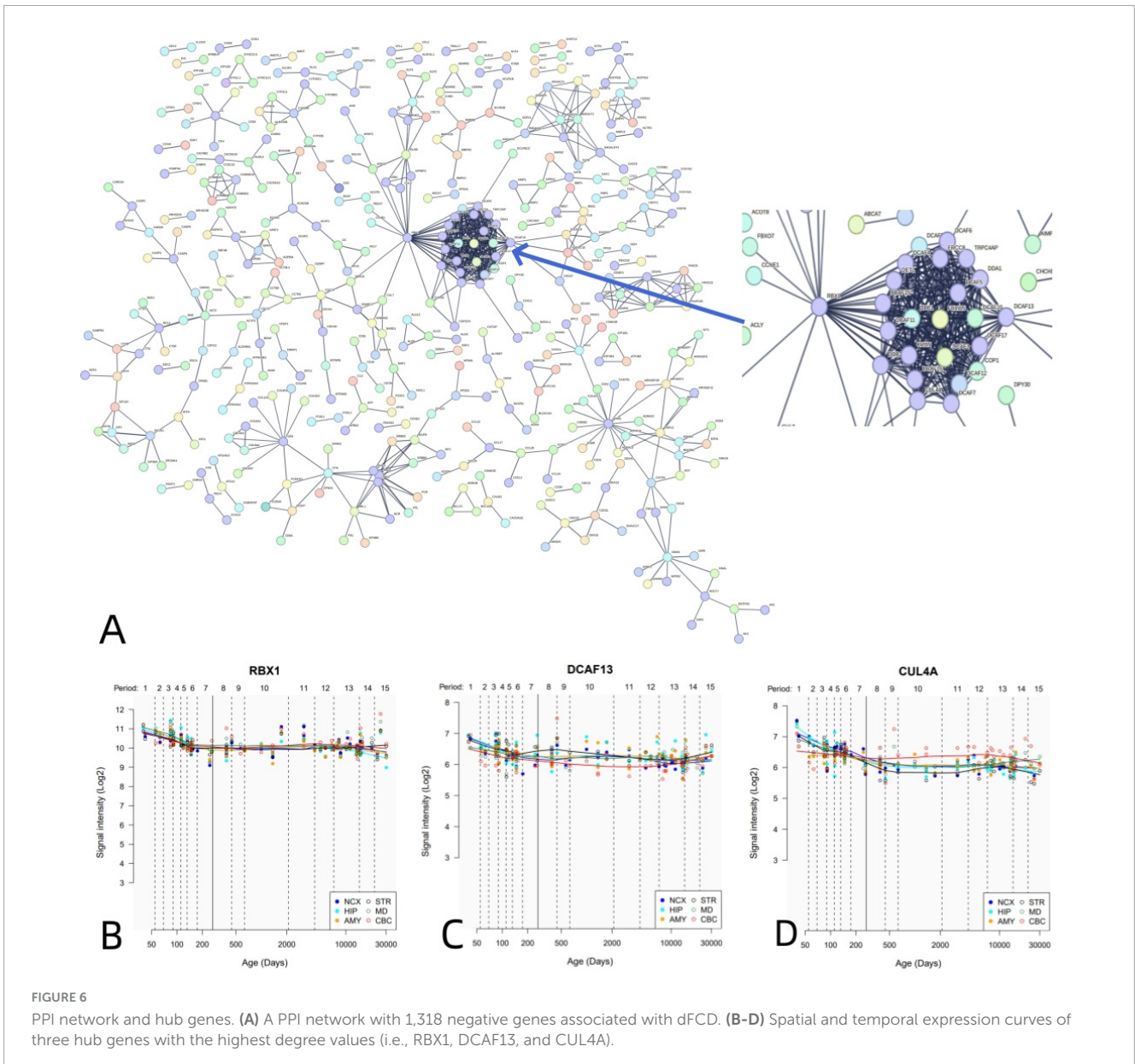


FIGURE 5 PPI network and hub genes. (A) A PPI network with 1,318 positive genes associated with dFCD. (B-D) Spatial and temporal expression curves of three hub genes with the highest degree values (i.e., RBX1, DDB2, and CBX2).

PLS + gene demonstrated particular expression in Purkinje neurons (Cb.Pcp2) located in the cerebellar cortex (Hirano, 2018), pivotal for integrating cerebellar inputs and outputs. The regular firing activity of Purkinje neurons is maintained through precise ion channel control (Raman and Bean, 1999), and ion channel dysregulation leads to perturbations in the intrinsic membrane excitability of Purkinje neurons, causing abnormal firing in Purkinje neurons (Bushart and Shakkottai, 2019; Cook et al., 2021; Huang and Shakkottai, 2023), which corresponds to the enrichment of these genes in ion channels. We did not find significant specific expression of PLS- genes at the cellular level. Furthermore, time-specific expression analyses, using predefined thresholds, did not reveal specific expression of dFCD-related genes at distinct developmental stages.

PPI analyses have revealed that dFCD-related genes can form a PPI network supported by functionally significant hub genes crucial for various biological processes. For instance, the RBX1 gene encodes RBX1 (RING box protein 1), essential for developmental processes. RBX1 suppression triggers the DNA damage response (DDR), resulting in G2-M arrest, senescence, and apoptosis (Jia et al., 2011). Another example is DDB2 (damage-specific DNA-binding protein 2), a component of the group E gene associated with dyschromic dry dermatosis, participating in the initiation of molecular ubiquitination within the ubiquitin ligase complex involving DDB1 and CUL4A (cullin 4A) (Stoyanova et al., 2009; Yan et al., 2011). DDB2 directly interacts with progesterin and adipoQ receptor 3 (PAQR3), facilitating PAQR3 ubiquitination, consequently enhancing PI3K/AKT axis signaling to ameliorate



insulin resistance and mitigate retinopathy in diabetic mice (Xiao et al., 2022).

Several limitations are evident in this study. Firstly, the gene expression data originated from the brains of six postmortem donors, while the neuroimaging data were obtained from 93 living participants (Zeng et al., 2012; Hawrylycz et al., 2015). To address the differential sources, we focused on genes displaying more conserved expression profiles by setting a DS threshold, facilitating our transcriptome-neuroimaging spatial correlation analysis. Secondly, due to limited gene expression data in the right hemisphere and notable variations between cortical and subcortical regions, only tissue samples from the left cerebral cortex were included, potentially introducing bias. Thirdly, oversampling in spatial correlation analyses is a common concern, which may inflate the rate of false positives. Lastly, gene identification related to dynamic functional connectivity density (dFCD) was achieved indirectly through spatial correlation analysis of transcriptional

neuroimaging, lacking direct experimental validation. Further exploration and validation through animal experiments are recommended for future studies.

## Conclusion

Our study identified altered dFCD variability in brain regions linked to visual and cognitive functions in DR patients. This was manifested by significantly lower dFCD variability in the left anterior cingulate gyrus, left supraoccipital gyrus, and right postcentral gyrus in DR group. Moreover, transcriptome-neuroimaging correlation analyses revealed a spatial association between these dFCD changes and the genes with unique functional profiles. These genes were enriched in biologically significant functions and pathways, specific to certain cells and brain areas. Our research offers novel understandings of the genetic

mechanisms influencing dFCD alterations in DR. The findings are also important for the diagnosis of DR and the discovery of potential therapeutic targets for DR.

## Data availability statement

The raw data supporting the conclusions of this article will be made available by the authors, without undue reservation.

## Ethics statement

The study protocol adhered to the Declaration of Helsinki and received approval from the Research Ethics Committee of Jiangxi Provincial People's Hospital. The studies were conducted in accordance with the local legislation and institutional requirements. The participants provided their written informed consent to participate in this study.

## Author contributions

Y-LZ: Conceptualization, Data curation, Formal Analysis, Funding acquisition, Project administration, Software, Supervision, Visualization, Writing – original draft, Writing – review & editing. HL: Conceptualization, Data curation, Formal Analysis, Funding acquisition, Resources, Supervision, Validation, Writing – original draft, Writing – review & editing. XH: Conceptualization, Data curation, Formal Analysis, Funding acquisition, Investigation,

Project administration, Resources, Validation, Visualization, Writing – original draft, Writing – review & editing.

## Funding

The author(s) declare that financial support was received for the research and/or publication of this article. This work was supported by the Natural Science Foundation of Jiangxi Province (20212BAB216058), Jiangxi Provincial Health Technology Project (202210012, 202310114, and 202410008), and Jiangxi Provincial traditional Chinese Technology Project (2022B840 and 2023A0138).

## Conflict of interest

The authors declare that the research was conducted in the absence of any commercial or financial relationships that could be construed as a potential conflict of interest.

## Publisher's note

All claims expressed in this article are solely those of the authors and do not necessarily represent those of their affiliated organizations, or those of the publisher, the editors and the reviewers. Any product that may be evaluated in this article, or claim that may be made by its manufacturer, is not guaranteed or endorsed by the publisher.

## References

- Arnatkeviciute, A., Fulcher, B. D., and Fornito, A. (2019). A practical guide to linking brain-wide gene expression and neuroimaging data. *Neuroimage* 189, 353–367. doi: 10.1016/j.neuroimage.2019.01.011
- Arnatkeviciute, A., Fulcher, B. D., Bellgrove, M. A., and Fornito, A. (2022). Imaging transcriptomics of brain disorders. *Biol. Psychiatry Glob. Open Sci.* 2, 319–331. doi: 10.1016/j.bpsgos.2021.10.002
- Aveira, C. A., Lin, C.-M., Abcouwer, S. F., Ambrósio, A. F., and Antonetti, D. A. (2010). TNF- $\alpha$  signals through PKC $\zeta$ /NF- $\kappa$ B to alter the tight junction complex and increase retinal endothelial cell permeability. *Diabetes* 59, 2872–2882. doi: 10.2337/db09-1606
- Bahtiyar, G., Gutterman, D., and Lebovitz, H. (2016). Heart failure: A major cardiovascular complication of diabetes mellitus. *Curr. Diab. Rep.* 16:116. doi: 10.1007/s11892-016-0809-4
- Bansal, S., Burman, A., and Tripathi, A. K. (2023). Advanced glycation end products: Key mediator and therapeutic target of cardiovascular complications in diabetes. *World J. Diabetes* 14, 1146–1162. doi: 10.4239/wjcd.v14.i8.1146
- Barber, A. J., Lieth, E., Khin, S. A., Antonetti, D. A., Buchanan, A. G., and Gardner, T. W. (1998). Neural apoptosis in the retina during experimental and human diabetes. *Early onset and effect of insulin.* *J. Clin. Invest.* 102, 783–791. doi: 10.1172/JCI2425
- Barkhof, F., Haller, S., and Rombouts, S. A. R. B. (2014). Resting-state functional MR imaging: A new window to the brain. *Radiology* 272, 29–49. doi: 10.1148/radiol.14132388
- Berkowitz, B. A., Bissig, D., Patel, P., Bhatia, A., and Roberts, R. (2012). Acute systemic 11-cis-retinal intervention improves abnormal outer retinal ion channel closure in diabetic mice. *Mol. Vis.* 18, 372–376.
- Biessels, G. J., and Despa, F. (2018). Cognitive decline and dementia in diabetes mellitus: Mechanisms and clinical implications. *Nat. Rev. Endocrinol.* 14, 591–604. doi: 10.1038/s41574-018-0048-7
- Bushart, D. D., and Shakkottai, V. G. (2019). Ion channel dysfunction in cerebellar ataxia. *Neurosci. Lett.* 688, 41–48. doi: 10.1016/j.neulet.2018.02.005
- Calhoun, V. D., Miller, R., Pearlson, G., and Adal, T. (2014). The chronectome: Time-varying connectivity networks as the next frontier in fMRI data discovery. *Neuron* 84, 262–274. doi: 10.1016/j.neuron.2014.10.015
- Casini, G., Catalani, E., Dal Monte, M., and Bagnoli, P. (2005). Functional aspects of the somatostatinergic system in the retina and the potential therapeutic role of somatostatin in retinal disease. *Histol. Histopathol.* 20, 615–632. doi: 10.14670/HH-20.615
- Chai, Y.-H., Han, Y.-P., Zhang, J.-Y., and Zhou, J.-B. (2024). Diabetic retinopathy and brain structure, cognition function, and dementia: A bidirectional mendelian randomization study. *J. Alzheimers Dis.* 97, 1211–1221. doi: 10.3233/JAD-231022
- Chenji, S., Jha, S., Lee, D., Brown, M., Seres, P., Mah, D., et al. (2016). Investigating default mode and sensorimotor network connectivity in amyotrophic lateral sclerosis. *PLoS One* 11:e0157443. doi: 10.1371/journal.pone.0157443
- Cho, H., and Sobrin, L. (2014). Genetics of diabetic retinopathy. *Curr. Diab. Rep.* 14:515. doi: 10.1007/s11892-014-0515-z
- Ciudin, A., Espinosa, A., Simó-Servat, O., Ruiz, A., Alegret, M., Hernández, C., et al. (2017). Type 2 diabetes is an independent risk factor for dementia conversion in patients with mild cognitive impairment. *J. Diabetes Complications* 31, 1272–1274. doi: 10.1016/j.jdiacomp.2017.04.018
- Cook, A. A., Fields, E., and Watt, A. J. (2021). Losing the beat: Contribution of purkinje cell firing dysfunction to disease, and its reversal. *Neuroscience* 462, 247–261. doi: 10.1016/j.neuroscience.2020.06.008
- Crosby-Nwaobi, R. R., Sivaprasad, S., Amiel, S., and Forbes, A. (2013). The relationship between diabetic retinopathy and cognitive impairment. *Diabetes Care* 36, 3177–3186. doi: 10.2337/dc12-2141

- Daruich, A., Matet, A., Moulin, A., Kowalczyk, L., Nicolas, M., Sellam, A., et al. (2018). Mechanisms of macular edema: Beyond the surface. *Prog. Retin. Eye Res.* 63, 20–68. doi: 10.1016/j.preteyeres.2017.10.006
- Edwards, S. L., Beesley, J., French, J. D., and Dunning, A. M. (2013). Beyond GWAS: Illuminating the dark road from association to function. *Am. J. Hum. Genet.* 93, 779–797. doi: 10.1016/j.ajhg.2013.10.012
- Eleftheriou, C. G., Ivanova, E., and Sagdullaev, B. T. (2020). Of neurons and pericytes: The neuro-vascular approach to diabetic retinopathy. *Vis. Neurosci.* 37:E005. doi: 10.1017/S0952523820000048
- Fornito, A., Arnatkevičiūtė, A., and Fulcher, B. D. (2019). Bridging the gap between connectome and transcriptome. *Trends Cogn. Sci.* 23, 34–50. doi: 10.1016/j.tics.2018.10.005
- Fornito, A., Zalesky, A., Bassett, D. S., Meunier, D., Ellison-Wright, I., Yücel, M., et al. (2011). Genetic influences on cost-efficient organization of human cortical functional networks. *J. Neurosci.* 31, 3261–3270. doi: 10.1523/JNEUROSCI.4858-10.2011
- Fox, M. D., and Raichle, M. E. (2007). Spontaneous fluctuations in brain activity observed with functional magnetic resonance imaging. *Nat. Rev. Neurosci.* 8, 700–711. doi: 10.1038/nrn2201
- Fox, M. D., Zhang, D., Snyder, A. Z., and Raichle, M. E. (2009). The global signal and observed anticorrelated resting state brain networks. *J. Neurophysiol.* 101, 3270–3283. doi: 10.1152/jn.90777.2008
- Grassi, M. A., Tikhomirov, A., Ramalingam, S., Below, J. E., Cox, N. J., and Nicolae, D. L. (2011). Genome-wide meta-analysis for severe diabetic retinopathy. *Hum. Mol. Genet.* 20, 2472–2481. doi: 10.1093/hmg/ddr121
- Hägg, S., Thorn, L. M., Putaala, J., Liebkind, R., Harjutsalo, V., Forsblom, C. M., et al. (2013). Incidence of stroke according to presence of diabetic nephropathy and severe diabetic retinopathy in patients with type 1 diabetes. *Diabetes Care* 36, 4140–4146. doi: 10.2337/dc13-0669
- Hawrylycz, M., Miller, J. A., Menon, V., Feng, D., Dolbear, T., Guillozet-Bongaarts, A. L., et al. (2015). Canonical genetic signatures of the adult human brain. *Nat. Neurosci.* 18, 1832–1844. doi: 10.1038/nn.4171
- Hirano, T. (2018). Purkinje neurons: Development, morphology, and function. *Cerebellum* 17, 699–700. doi: 10.1007/s12311-018-0985-7
- Huang, H., and Shakkottai, V. G. (2023). Targeting ion channels and purkinje neuron intrinsic membrane excitability as a therapeutic strategy for cerebellar ataxia. *Life (Basel)* 13:1350. doi: 10.3390/life13061350
- Huang, X., Tong, Y., Qi, C.-X., Dan, H.-D., Deng, Q.-Q., and Shen, Y. (2020). Large-scale neuronal network dysfunction in diabetic retinopathy. *Neural Plast.* 2020:6872508. doi: 10.1155/2020/6872508
- Huang, X., Tong, Y., Qi, C.-X., Xu, Y.-T., Dan, H.-D., and Shen, Y. (2019). Disrupted topological organization of human brain connectome in diabetic retinopathy patients. *Neuropsychiatr. Dis. Treat.* 15, 2487–2502. doi: 10.2147/NDT.S214325
- Huang, X., Wen, Z., Qi, C.-X., Tong, Y., and Shen, Y. (2021a). Dynamic changes of amplitude of low-frequency fluctuations in patients with diabetic retinopathy. *Front. Neurol.* 12:611702. doi: 10.3389/fneur.2021.611702
- Huang, X., Xie, B.-J., Qi, C.-X., Tong, Y., and Shen, Y. (2021b). Abnormal intrinsic functional network hubs in diabetic retinopathy patients. *Neuroreport* 32, 498–506. doi: 10.1097/WNR.0000000000001620
- Hull, J. M., and Isom, L. L. (2018). Voltage-gated sodium channel  $\beta$  subunits: The power outside the pore in brain development and disease. *Neuropharmacology* 132, 43–57. doi: 10.1016/j.neuropharm.2017.09.018
- Hutchison, R. M., Womelsdorf, T., Allen, E. A., Bandettini, P. A., Calhoun, V. D., Corbetta, M., et al. (2013). Dynamic functional connectivity: Promise, issues, and interpretations. *Neuroimage* 80, 360–378. doi: 10.1016/j.neuroimage.2013.05.079
- Jackson, P. L., Brunet, E., Meltzoff, A. N., and Decety, J. (2006). Empathy examined through the neural mechanisms involved in imagining how I feel versus how you feel pain. *Neuropsychologia* 44, 752–761. doi: 10.1016/j.neuropsychologia.2005.07.015
- Jia, L., Bickel, J. S., Wu, J., Morgan, M. A., Li, H., Yang, J., et al. (2011). RBX1 (RING box protein 1) E3 ubiquitin ligase is required for genomic integrity by modulating DNA replication licensing proteins. *J. Biol. Chem.* 286, 3379–3386. doi: 10.1074/jbc.M110.188425
- Kim, J., Jensen, A., Ko, S., Raghavan, S., Phillips, L. S., Hung, A., et al. (2022). Systematic heritability and heritability enrichment analysis for diabetes complications in UK Biobank and ACCORD studies. *Diabetes* 71, 1137–1148. doi: 10.2337/db21-0839
- Kumar, P., Kumar, D., Jha, S. K., Jha, N. K., and Ambasta, R. K. (2016). Ion Channels in neurological disorders. *Adv. Protein Chem. Struct. Biol.* 103, 97–136. doi: 10.1016/bs.apcsb.2015.10.006
- Kwa, V. I. H., van der Sande, J. J., Stam, J., Tijmes, N., Vrooland, J. L., Amsterdam Vascular, et al. (2002). Retinal arterial changes correlate with cerebral small-vessel disease. *Neurology* 59, 1536–1540. doi: 10.1212/01.wnl.0000033093.16450.5c
- Lee, Y.-J., Jeon, H.-Y., Lee, A.-J., Kim, M., and Ha, K.-S. (2022). Dopamine ameliorates hyperglycemic memory-induced microvascular dysfunction in diabetic retinopathy. *FASEB J.* 36:e22643. doi: 10.1096/fj.202200865R
- Leslie, R. D., and Pyke, D. A. (1982). Diabetic retinopathy in identical twins. *Diabetes* 31, 19–21. doi: 10.2337/diab.31.1.19
- Li, J., Duan, X., Cui, Q., Chen, H., and Liao, W. (2019). More than just statics: Temporal dynamics of intrinsic brain activity predicts the suicidal ideation in depressed patients. *Psychol. Med.* 49, 852–860. doi: 10.1017/S0033291718001502
- Liao, W., Li, J., Ji, G.-J., Wu, G.-R., Long, Z., Xu, Q., et al. (2019). Endless fluctuations: Temporal dynamics of the amplitude of low frequency fluctuations. *IEEE Trans. Med. Imaging* 38, 2523–2532. doi: 10.1109/TMI.2019.2904555
- Liao, X.-L., Yuan, Q., Shi, W.-Q., Li, B., Su, T., Lin, Q., et al. (2019). Altered brain activity in patients with diabetic retinopathy using regional homogeneity: A resting-state fMRI study. *Endocr. Pract.* 25, 320–327. doi: 10.4158/EP-2018-0517
- Lopes de Faria, J. B., Silva, K. C., Lopes, and de Faria, J. M. (2011). The contribution of hypertension to diabetic nephropathy and retinopathy: The role of inflammation and oxidative stress. *Hypertens Res.* 34, 413–422. doi: 10.1038/hr.2010.263
- Lv, H., Wang, Z., Tong, E., Williams, L. M., Zaharchuk, G., Zeineh, M., et al. (2018). Resting-state functional MRI: Everything that nonexperts have always wanted to know. *AJNR Am. J. Neuroradiol.* 39, 1390–1399. doi: 10.3174/ajnr.A5527
- Moody, W. J., and Bosma, M. M. (2005). Ion channel development, spontaneous activity, and activity-dependent development in nerve and muscle cells. *Physiol. Rev.* 85, 883–941. doi: 10.1152/physrev.00017.2004
- Murphy, K., Birn, R. M., Handwerker, D. A., Jones, T. B., and Bandettini, P. A. (2009). The impact of global signal regression on resting state correlations: Are anti-correlated networks introduced? *Neuroimage* 44, 893–905. doi: 10.1016/j.neuroimage.2008.09.036
- Pang, Y., Cui, Q., Duan, X., Chen, H., Zeng, L., Zhang, Z., et al. (2017). Extraversion modulates functional connectivity hubs of resting-state brain networks. *J. Neuropsychol.* 11, 347–361. doi: 10.1111/jnp.12090
- Pardo, J. V., Pardo, P. J., Janer, K. W., and Raichle, M. E. (1990). The anterior cingulate cortex mediates processing selection in the Stroop attentional conflict paradigm. *Proc. Natl. Acad. Sci. U S A.* 87, 256–259. doi: 10.1073/pnas.87.1.256
- Pereda, A. E. (2014). Electrical synapses and their functional interactions with chemical synapses. *Nat. Rev. Neurosci.* 15, 250–263. doi: 10.1038/nrn3708
- Qi, C.-X., Huang, X., and Shen, Y. (2020). Altered intrinsic brain activities in patients with diabetic retinopathy using amplitude of low-frequency fluctuation: A resting-state fMRI study. *Diabetes Metab. Syndr. Obes.* 13, 2833–2842. doi: 10.2147/DMSO.S259476
- Raman, I. M., and Bean, B. P. (1999). Ionic currents underlying spontaneous action potentials in isolated cerebellar Purkinje neurons. *J. Neurosci.* 19, 1663–1674. doi: 10.1523/JNEUROSCI.19-05-01663.1999
- Ringach, D. L., Hawken, M. J., and Shapley, R. (1996). Binocular eye movements caused by the perception of three-dimensional structure from motion. *Vision Res.* 36, 1479–1492. doi: 10.1016/0042-6989(95)00285-5
- Sanahuja, J., Alonso, N., Diez, J., Ortega, E., Rubinat, E., Traveset, A., et al. (2016). Increased burden of cerebral small vessel disease in patients with type 2 diabetes and retinopathy. *Diabetes Care* 39, 1614–1620. doi: 10.2337/dc15-2671
- Shi, W.-Q., Zhang, M.-X., Tang, L.-Y., Ye, L., Zhang, Y.-Q., Lin, Q., et al. (2022). Altered spontaneous brain activity patterns in patients with diabetic retinopathy using amplitude of low-frequency fluctuation. *World J. Diabetes* 13, 97–109. doi: 10.4239/wjdv13.i2.97
- Smith, R. S., and Walsh, C. A. (2020). Ion channel functions in early brain development. *Trends Neurosci.* 43, 103–114. doi: 10.1016/j.tins.2019.12.004
- Stoyanova, T., Roy, N., Kopanja, D., Bagchi, S., and Raychaudhuri, P. (2009). DDB2 decides cell fate following DNA damage. *Proc. Natl. Acad. Sci. U S A.* 106, 10690–10695. doi: 10.1073/pnas.0812254106
- Tam, V., Patel, N., Turcotte, M., Bossé, Y., Paré, G., and Meyre, D. (2019). Benefits and limitations of genome-wide association studies. *Nat. Rev. Genet.* 20, 467–484. doi: 10.1038/s41576-019-0127-1
- Teo, Z. L., Tham, Y.-C., Yu, M., Chee, M. L., Rim, T. H., Cheung, N., et al. (2021). Global prevalence of diabetic retinopathy and projection of burden through 2045: Systematic review and meta-analysis. *Ophthalmology* 128, 1580–1591. doi: 10.1016/j.ophtha.2021.04.027
- Ting, D. S. W., Cheung, G. C. M., and Wong, T. Y. (2016). Diabetic retinopathy: Global prevalence, major risk factors, screening practices and public health challenges: A review. *Clin. Exp. Ophthalmol.* 44, 260–277. doi: 10.1111/ceo.12696
- Tomasi, D., and Volkow, N. D. (2010). Functional connectivity density mapping. *Proc. Natl. Acad. Sci. U S A.* 107, 9885–9890. doi: 10.1073/pnas.1001414107
- Tomasi, D., Shokri-Kojori, E., and Volkow, N. D. (2016). High-resolution functional connectivity density: Hub locations, sensitivity, specificity, reproducibility, and reliability. *Cereb. Cortex* 26, 3249–3259. doi: 10.1093/cercor/bhv171
- Tzourio-Mazoyer, N., Landeau, B., Papathanassiou, D., Crivello, F., Etard, O., Delcroix, N., et al. (2002). Automated anatomical labeling of activations in SPM using a macroscopic anatomical parcellation of the MNI MRI single-subject brain. *Neuroimage* 15, 273–289. doi: 10.1006/nimg.2001.0978
- van de Kreeke, J. A., Nguyen, H. T., Konijnenberg, E., Tomassen, J., den Braber, A., Ten Kate, M., et al. (2018). Retinal and cerebral microvasculopathy: Relationships and

- their genetic contributions. *Invest. Ophthalmol. Vis. Sci.* 59, 5025–5031. doi: 10.1167/iov.18-25341
- Van Dijk, K. R. A., Sabuncu, M. R., and Buckner, R. L. (2012). The influence of head motion on intrinsic functional connectivity MRI. *Neuroimage* 59, 431–438. doi: 10.1016/j.neuroimage.2011.07.044
- van Duinkerken, E., Ijzerman, R. G., Klein, M., Moll, A. C., Snoek, F. J., Scheltens, P., et al. (2016). Disrupted subject-specific gray matter network properties and cognitive dysfunction in type 1 diabetes patients with and without proliferative retinopathy. *Hum. Brain Mapp.* 37, 1194–1208. doi: 10.1002/hbm.23096
- Wang, K., Jiang, T., Yu, C., Tian, L., Li, J., Liu, Y., et al. (2008). Spontaneous activity associated with primary visual cortex: A resting-state fMRI study. *Cereb. Cortex* 18, 697–704. doi: 10.1093/cercor/bhm105
- Wessels, A. M., Simsek, S., Remijnse, P. L., Veltman, D. J., Biessels, G. J., Barkhof, F., et al. (2006). Voxel-based morphometry demonstrates reduced grey matter density on brain MRI in patients with diabetic retinopathy. *Diabetologia* 49, 2474–2480. doi: 10.1007/s00125-006-0283-7
- Wondmeneh, T. G., and Mohammed, J. A. (2024). Prevalence of diabetic retinopathy and its associated risk factors among adults in Ethiopia: A systematic review and meta-analysis. *Sci. Rep.* 14:28266. doi: 10.1038/s41598-024-78596-9
- Wong, T. Y., Cheung, C. M. G., Larsen, M., Sharma, S., and Simó, R. (2016). Diabetic retinopathy. *Nat. Rev. Dis. Primers* 2:16012. doi: 10.1038/nrdp.2016.12
- Xiao, H., Sun, X., Lin, Z., Yang, Y., Zhang, M., Xu, Z., et al. (2022). Gentiopicroside targets PAQR3 to activate the PI3K/AKT signaling pathway and ameliorate disordered glucose and lipid metabolism. *Acta Pharm. Sin. B* 12, 2887–2904. doi: 10.1016/j.apsb.2021.12.023
- Xu, H.-Z., Song, Z., Fu, S., Zhu, M., and Le, Y.-Z. (2011). RPE barrier breakdown in diabetic retinopathy: Seeing is believing. *J. Ocul. Biol. Dis. Infor.* 4, 83–92. doi: 10.1007/s12177-011-9068-4
- Xu, R.-S. (2015). Pathogenesis of diabetic cerebral vascular disease complication. *World J. Diabetes* 6, 54–66. doi: 10.4239/wjdv6.i1.54
- Xue, K., Liang, S., Yang, B., Zhu, D., Xie, Y., Qin, W., et al. (2022). Local dynamic spontaneous brain activity changes in first-episode, treatment-naïve patients with major depressive disorder and their associated gene expression profiles. *Psychol. Med.* 52, 2052–2061. doi: 10.1017/S0033291720003876
- Yan, C.-G., Wang, X.-D., Zuo, X.-N., and Zang, Y.-F. (2016). DPABI: Data processing & analysis for (Resting-State) brain imaging. *Neuroinformatics* 14, 339–351. doi: 10.1007/s12021-016-9299-4
- Yan, Y., Zhang, X., and Legerski, R. J. (2011). Artemis interacts with the Cul4A-DDB1DDB2 ubiquitin E3 ligase and regulates degradation of the CDK inhibitor p27. *Cell Cycle* 10, 4098–4109. doi: 10.4161/cc.10.23.18227
- Zeng, H., Shen, E. H., Hohmann, J. G., Oh, S. W., Bernard, A., Royall, J. J., et al. (2012). Large-scale cellular-resolution gene profiling in human neocortex reveals species-specific molecular signatures. *Cell* 149, 483–496. doi: 10.1016/j.cell.2012.02.052
- Zhang, C., Cai, H., Xu, X., Li, Q., Li, X., Zhao, W., et al. (2022). Genetic architecture underlying differential resting-state functional connectivity of subregions within the human visual cortex. *Cereb. Cortex* 32, 2063–2078. doi: 10.1093/cercor/bhab335
- Zhang, X., Gao, Y., Zhou, Z., Wang, J., Zhou, Q., and Li, Q. (2010). Familial clustering of diabetic retinopathy in Chongqing, China, type 2 diabetic patients. *Eur. J. Ophthalmol.* 20, 911–918. doi: 10.1177/112067211002000516
- Zhang, Z., Liao, M., Yao, Z., Hu, B., Xie, Y., Zheng, W., et al. (2017). Frequency-specific functional connectivity density as an effective biomarker for adolescent generalized anxiety disorder. *Front. Hum. Neurosci.* 11:549. doi: 10.3389/fnhum.2017.00549
- Zhao, B., Huang, J., Lou, X., Yao, K., Ye, M., Mou, Q., et al. (2022). Endothelial CYP2J2 overexpression restores the BRB via METTL3-mediated ANXA1 upregulation. *FASEB J.* 36:e22619. doi: 10.1096/fj.202201061RR
- Zhu, H., Zhang, W., Zhao, Y., Shu, X., Wang, W., Wang, D., et al. (2018). GSK3 $\beta$ -mediated tau hyperphosphorylation triggers diabetic retinal neurodegeneration by disrupting synaptic and mitochondrial functions. *Mol. Neurodegener.* 13:62. doi: 10.1186/s13024-018-0295-z